# Fermi Surface in Tungsten

L. F. MATTHEISS
*Bell Telephone Laboratories, Murray Hill, New Jersey*
(Received 29 April 1965)

The results of nonrelativistic, augmented-plane-wave energy-band calculations have been used to calculate the Fermi surface in body-centered cubic tungsten, neglecting spin-orbit coupling. The resulting Fermi surface is very similar to one proposed earlier by Lomer for group-VI transition metals and agrees qualitatively with the available experimental results. Spin-orbit coupling is found to have little effect on the basic Fermi-surface topology in tungsten and its consequences can be understood qualitatively in terms of a simplified tight-binding calculation. Within the energy range of the tungsten 5*d* bands, the electronic density of states contains four distinct peaks, three of which lie below the tungsten Fermi energy. Assuming a rigid-band model, the present energy-band results have been used to predict the Fermi surface in the group-V transition metals.

## I. INTRODUCTION

TUNGSTEN is one of the first transition metals to become available in high-purity, single-crystal form. As a result, most of the experimental techniques for studying the electronic properties of metals have been applied to tungsten. These have included measurements of the anomalous skin effect,[1] magnetoresistance,[2–5] the magnetoacoustic effect,[6] the de Haas–van Alphen effect,[7–9] Azbel'-Kaner cyclotron resonance,[10,11] and the Gantmakher size effect.[12] The majority of the experimental results, as well as their interpretation, remain unpublished. The objectives of the present investigation are: (i) to calculate a model Fermi surface for body-centered cubic tungsten from the results of nonrelativistic augmented-plane-wave (APW) energy-band calculations; (ii) to determine semiempirically the effects of spin-orbit coupling on this model Fermi surface; (iii) to compare this calculated Fermi surface and other electronic properties with the available experimental results.

Interest in the energy-band structure of tungsten dates back to calculations by Manning and Chodorow[13] in the late thirties using the cellular method. More recently, a Fermi surface for the chromium-group metals has been proposed by Lomer.[14] This model Fermi surface has been based primarily on Wood's APW calculations for iron.[15] Recently, Lomer has revised this model Fermi surface (Lomer II) and limited its application to molybdenum.[16] This revised Fermi surface is sketched in Fig. 1. It consists of two main, closed surfaces that have been described as an electron "jack" centered at the origin of the Brillouin-zone $\Gamma$ and hole "octahedra" at the symmetry points $H$. The electron "jack" consists of an octahedral body connected to six ball-like protrusions along the $\langle 100\rangle$ or $\bar{\Gamma}\bar{H}$ directions. Within the "necks" which join the octahedral body to the balls are the electron "lenses." Neglecting spin-orbit coupling, these "lenses" contact the "necks" in the (100) and (110) planes. In this approximation, the electron "jack" at $\Gamma$ contacts the hole "octahedra" at $H$ along the $\langle 100\rangle$ directions in the Brillouin zone. Finally, this model predicts small hole pockets at $N$. In his original model (Lomer I), Lomer overlooked the presence of the ball-like protrusions on the electron surface at $\Gamma$ and assumed that this surface tapered smoothly along the $\langle 100\rangle$ directions.

In the present investigation, two fairly complete APW calculations have been carried out for tungsten, using slightly different crystal potentials. The results of these two calculations differ mainly in the calculated *s-d* energy separation and the 5*d* bandwidths. These 5*d* band widths vary from approximately 0.8 to 1.0 Ry, the latter value agreeing quite well with that found by Manning and Chodorow.[13] The present energy-band results are quite similar to those obtained by Manning and Chodorow, except that they found that the bottom of the 6*s* conduction band was above the bottom of the 5*d* bands while the present results indicate that it lies about 0.1 Ry below the 5*d* bands.

The Fermi surface for tungsten which results from the present nonrelativistic APW calculations agrees qualitatively with the Lomer II model shown in Fig. 1.

[1] E. Fawcett and D. Griffiths, J. Phys. Chem. Solids **23**, 1631 (1962).
[2] E. Justi and H. Scheffers, Physik. Z. **37**, 700 (1936).
[3] E. Fawcett, Phys. Rev. Letters **7**, 370 (1961); E. Fawcett, Phys. Rev. **128**, 154 (1962).
[4] N. V. Volkenshtein, V. N. Kachinskii, and L. S. Starostina, Zh. Eksperim i Teor. Fiz. **45**, 43 (1963) [English transl.: Soviet Phys.—JETP **18**, 32 (1964)].
[5] E. Fawcett and W. A. Reed, Phys. Rev. **134**, A723 (1964).
[6] J. A. Rayne and H. Sell, Phys. Rev. Letters **8**, 199 (1962); J. A. Rayne, Phys. Rev. **133**, A1104 (1964); C. K. Jones and J. A. Rayne, Proceedings of the Ninth International Conference on Low Temperature Physics, Columbus, 1964 (to be published).
[7] G. B. Brandt and J. A. Rayne, Phys. Letters **3**, 148 (1962); Phys. Rev. **132**, 1945 (1963).
[8] D. Sparlin and J. A. Marcus, Bull. Am. Phys. Soc. **8**, 258 (1963); **9**, 250 (1964).
[9] R. F. Girvan and A. V. Gold (private communication).
[10] E. Fawcett and W. M. Walsh, Jr., Phys. Rev. Letters **8**, 476 (1962).
[11] W. M. Walsh, Jr., Phys. Rev. Letters **12**, 161 (1964).
[12] W. M. Walsh, Jr. and C. C. Grimes, Phys. Rev. Letters **13**, 523 (1964).
[13] M. F. Manning and M. I. Chodorow, Phys. Rev. **56**, 789 (1939).
[14] W. M. Lomer, Proc. Phys. Soc. (London) **80**, 489 (1962).
[15] J. H. Wood, Phys. Rev. **126**, 517 (1962).
[16] W. M. Lomer, Proc. Phys. Soc. (London) **84**, 327 (1964).

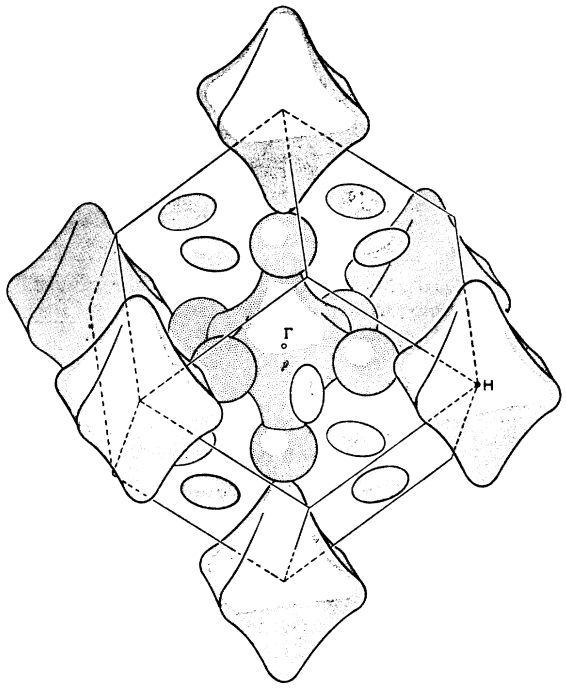


FIG. 1. A three-dimensional stretch of Lomer's revised Fermi surface for chromium-group metals.

However, there has been some reluctance to apply the Lomer II model Fermi surface for chromium-group metals to tungsten, mainly because the low-field de Haas–van Alphen results for molybdenum and tungsten differ significantly.[7] This has been attributed to an enhanced spin-orbit coupling in the latter element.[7,16] However, the data from de Haas–van Alphen measurements on tungsten by Sparlin and Marcus[8] and their interpretation by Sparlin[17] are consistent with the Lomer II model Fermi surface. According to Sparlin, the Fermi surfaces for molybdenum and tungsten differ in two respects: First, the dimensions of the hole pockets at $N$ are smaller in tungsten than in molybdenum. Second, the extremal areas for orbits associated with the "lenses" in tungsten have not been observed, whereas they have been measured in molybdenum. Sparlin and Marcus have inferred the re-entrant nature of the electron surface at Γ from their analysis of the de Haas–van Alphen results and introduced the term electron "jack."

The most striking experimental verification of the Lomer II model Fermi surface in tungsten is a consequence of the size-effect experiments by Walsh and Grimes,[12] who mapped out the extremal linear dimensions of portions of the electron "jack" and the entire hole "octahedron" in a (110) plane. Walsh and Grimes have shown that the electron "jack" at Γ fails to contact the hole "octahedra" at $H$, as the nonrelativistic energy-band results predict. Rather, these electron and hole surfaces are separated by a gap equal approximately to 5% the $\Gamma\bar{H}$ distance. This splitting has been attributed to the effects of spin-orbit coupling.[18] Using a simplified model, it has been possible to use the measured separation between the electron "jack" and hole "octahedra" to estimate the 5$d$ spin-orbit coupling parameter $\xi_{5d}$ in metallic tungsten to be approximately 0.03 Ry (0.4 eV). Another consequence of spin-orbit coupling is that it could cause the "lenses" to disappear in tungsten.

A brief description of the present calculation is contained in the following section, including a discussion of the approximate crystal potentials which have been used. The results of these APW calculations are presented in Sec. III, including for each calculation, $E(\mathbf{k})$ curves along symmetry directions in the Brillouin zone, a density-of-states, and the resulting Fermi surface. In Sec. IV, a brief description of the simplified model used to estimate the effects of spin-orbit coupling is presented. In Sec. V, a Fermi-surface model for the group-V transition metals vanadium (V), niobium (Nb), and tantalum (Ta) is proposed. The final section contains a discussion of the present energy-band results and comparisons with experiment.

## II. DESCRIPTION OF THE CALCULATION

The present nonrelativistic energy-band calculations for body-centered cubic tungsten have been carried out using the APW method,[19] as programmed for the IBM computers by Wood.[15] The crystal potential has been approximated by a "muffin-tin" potential, which is calculated by superimposing atomic potentials in a manner that has been described earlier in connection with an energy-band study of the 3$d$ transition series.[20] Exchange has been treated approximately using Slater's free-electron exchange approximation.[21]

Instead of using the self-consistent atomic Hartree-Fock charge densities that have been used previously in calculations for the 3$d$ transition series, the present calculations utilize potentials which have been obtained from Hartree-Fock-Slater charge densities, as provided by Herman and Skillman.[22] Unpublished calculations by the author indicate that equivalent results are obtained in the 3$d$ transition series using potentials which are derived from either atomic Hartree-Fock or Hartree-Fock-Slater charge densities.

The potentials used in the present calculations have been obtained using an assumed atomic configuration of $(5d)^5(6s)^1$ for tungsten, which is probably close to that in the solid. Two fairly complete calculations have

[17] D. M. Sparlin, thesis, Northwestern University, 1964 (unpublished).

[18] L. F. Mattheiss and R. E. Watson, Phys. Rev. Letters **13**, 526 (1964).

[19] J. C. Slater, Phys. Rev. **51**, 846 (1937).

[20] L. F. Mattheiss, Phys. Rev. **134**, A970 (1964).

[21] J. C. Slater, Phys. Rev. **81**, 385 (1951).

[22] F. Herman and S. Skillman, *Atomic Structure Calculations* (Prentice-Hall, Inc., Englewood Cliffs, New Jersey, 1963).

TABLE I. An abbreviated tabulation of the potentials used in the present calculations for tungsten. The radial distance $r$ is tabulated in terms of $r/r_0$ (where $r_0=0.005272$ a.u.) and $V(r)$ is in Ry. For both potentials, the APW sphere radius $R_s=2.59$ a.u.; the constant value of the potential between the APW spheres equals 1.466 and 1.181 Ry for $V_1$ and $V_2$, respectively.

| $r/r_0$ | $-V_1(r)$ | $-V_2(r)$ |
|---|---|---|
| 1 | 27256.823 | 27211.528 |
| 2 | 13229.229 | 13194.117 |
| 3 | 8568.264 | 8540.645 |
| 4 | 6248.878 | 6226.470 |
| 6 | 3950.230 | 3933.161 |
| 8 | 2818.407 | 2803.394 |
| 10 | 2149.628 | 2136.018 |
| 12 | 1710.687 | 1698.456 |
| 16 | 1174.998 | 1165.263 |
| 20 | 865.262 | 857.146 |
| 24 | 666.864 | 659.589 |
| 28 | 530.645 | 523.922 |
| 36 | 358.680 | 353.076 |
| 44 | 257.127 | 252.636 |
| 52 | 191.808 | 188.103 |
| 60 | 147.461 | 144.138 |
| 76 | 92.926 | 89.944 |
| 92 | 62.301 | 59.723 |
| 108 | 43.921 | 41.796 |
| 124 | 32.750 | 30.523 |
| 156 | 19.067 | 17.849 |
| 188 | 12.350 | 11.368 |
| 220 | 8.505 | 7.670 |
| 252 | 6.121 | 5.408 |
| 316 | 3.527 | 3.009 |
| 380 | 2.310 | 1.920 |
| 444 | 1.727 | 1.408 |
| 508 | 1.483 | 1.197 |

been carried through using two slightly different potentials, $V_1(r)$ and $V_2(r)$. These potentials differ only in the exchange contribution to the potential. In $V_2(r)$, the exchange potential in $V_1(r)$ has been reduced by 30%. This has been done in order to vary the $6s$-$5d$ energy separation in the simplest possible manner without modifying the potential drastically.

An abbreviated tabulation of the two potentials $V_1(r)$ and $V_2(r)$ which have been used in the present calculations for tungsten is presented in Table I. In this table, the radial distance $r$ is tabulated in terms of $r/r_0$, where $r_0=0.005272$ atomic units (a.u.) for tungsten. This radial mesh corresponds to the one used by Herman and Skillman,[22] being proportional to the inverse cube-root of the atomic number $Z$.

The lattice constant for tungsten which has been used in these calculations is the room-temperature value tabulated by Pearson[23] of 5.9811 a.u. (3.1651 Å). The lattice constant at 4.2°K has been estimated to be approximately 5.973 a.u. (3.161 Å),[12] using the thermal-expansion data of Nix and MacNair.[24]

## III. RESULTS

The Brillouin zone for the body-centered cubic Bravais lattice is shown in Fig. 2. In this figure as well

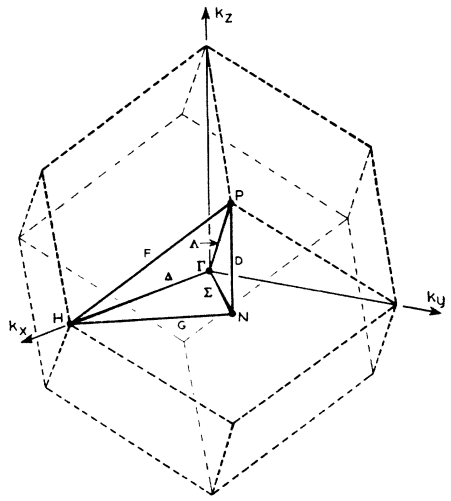


FIG. 2. The Brillouin zone for the body-centered cubic structure with symmetry points and lines labeled in accordance with the standard notation.

as in the following discussions, the notation due to Bouckaert, Smoluchowski, and Wigner[25] is used to label symmetry points and lines and the corresponding irreducible representations.

Two extensive APW calculations have been carried out for tungsten using the potentials $V_1(r)$ and $V_2(r)$ of Table I. The results of these calculations, which will be referred to either as $W_1$ and $W_2$ or $E_1(\mathbf{k})$ and $E_2(\mathbf{k})$, are shown in Figs. 3 and 4, respectively. Here, the energy bands $E_1(\mathbf{k})$ and $E_2(\mathbf{k})$ are plotted along symmetry directions in the Brillouin zone for tungsten. These APW results have been obtained at a total of 55 points in 1/48 of the Brillouin zone. The $W_1$ results are listed in Table II. The calculations have been carried out for $\mathbf{k}$ values which are distributed on a uniform mesh in the Brillouin zone such that the entire zone is subdivided into 1024 cubic subzones, each having edge dimensions $(\pi/4a)$.

The $5d$-band states are readily distinguished in Figs. 3 and 4. At the symmetry points, they correspond to the following states: $\Gamma_{12}$, $\Gamma_{25'}$; $H_{25'}$, $H_{12}$; $N_3$, $N_4$, $N_1$, $N_2$, $N_1$; $P_3$, $P_4$. It is clear from Fig. 4 that the $5d$ bandwidth is approximately 0.8 Ry. The state with $\Gamma_1$ symmetry represents the bottom of the $6s$ conduction band in both cases, while $N_{1'}$ represents a $6p$-type state. The ordering of states at symmetry points in the Brillouin zone in Figs. 3 and 4 is identical with that obtained by Wood for iron,[15] who found a $3d$ bandwidth slightly less than 0.5 Ry. The main differences between the results shown in Figs. 3 and 4 are the $5d$ bandwidth and the relative position of $E(N_{1'})$ with respect to the Fermi energy.

The energy-band results can be used to calculate a density-of-states for tungsten. However, due to the

[23] W. B. Pearson, *A Handbook of Lattice Spacings and Structures of Metals and Alloys* (Pergamon Press, Inc., New York, 1958).
[24] F. C. Nix and D. MacNair, Phys. Rev. **61**, 74 (1942).
[25] L. P. Bouckaert, R. Smoluchowski, and E. Wigner, Phys. Rev. **50**, 58 (1936).

TABLE II. Energy-band results for tungsten obtained using the potential $V_1(r)$ of Table I. Energies are in Ry, the zero of energy coinciding with the constant potential between the APW spheres, 1.466 Ry. The eigenvalues are identified using the notation of Bouckaert, Smoluchowski, and Wigner.

| $4(a/\pi)\mathbf{k}$ | Band 1 | Band 2 | Band 3 | Band 4 | Band 5 | Band 6 |
|---|---|---|---|---|---|---|
| $\Gamma(0,0,0)$ | 1 0.341 | 25′ 0.746 | 25′ 0.746 | 25′ 0.746 | 12 0.957 | 12 0.957 |
| $\Delta(1,0,0)$ | 1 0.366 | 5 0.745 | 5 0.745 | 2′ 0.759 | 2 0.920 | 1 0.973 |
| $\Delta(2,0,0)$ | 1 0.434 | 5 0.746 | 5 0.746 | 2′ 0.795 | 2 0.828 | 1 1.013 |
| $\Delta(3,0,0)$ | 1 0.517 | 2 0.717 | 5 0.762 | 5 0.762 | 2′ 0.850 | 1 1.067 |
| $\Delta(4,0,0)$ | 1 0.571 | 2 0.610 | 5 0.804 | 5 0.804 | 2′ 0.923 | 1 1.131 |
| $\Delta(5,0,0)$ | 2 0.520 | 1 0.552 | 5 0.877 | 5 0.877 | 2′ 1.006 | 1 1.225 |
| $\Delta(6,0,0)$ | 2 0.452 | 1 0.484 | 5 0.981 | 5 0.981 | 2′ 1.086 | 1 1.356 |
| $\Delta(7,0,0)$ | 2 0.410 | 1 0.421 | 5 1.099 | 5 1.099 | 2′ 1.147 | 1 1.49 |
| $H(8,0,0)$ | 12 0.396 | 12 0.396 | 25 1.169 | 25′ 1.169 | 25′ 1.169 | 15 1.554 |
| $\Sigma(1,1,0)$ | 1 0.389 | 2 0.716 | 1 0.737 | 3 0.797 | 1 0.923 | 4 0.960 |
| (2,1,0) | + 0.448 | − 0.699 | + 0.726 | − 0.854 | + 0.871 | + 0.997 |
| (3,1,0) | + 0.514 | + 0.695 | − 0.704 | + 0.831 | − 0.923 | + 1.057 |
| (4,1,0) | + 0.551 | + 0.629 | − 0.737 | + 0.844 | − 1.002 | + 1.142 |
| (5,1,0) | + 0.521 | + 0.573 | − 0.803 | + 0.867 | − 1.085 | + 1.260 |
| (6,1,0) | + 0.467 | + 0.503 | − 0.898 | + 0.938 | − 1.154 | + 1.41 |
| $G(7,1,0)$ | 1 0.428 | 4 0.441 | 3 1.011 | 1 1.038 | 2 1.179 | 4 1.538 |
| $\Sigma(2,2,0)$ | 1 0.473 | 2 0.655 | 1 0.729 | 1 0.927 | 3 0.939 | 4 0.976 |
| (3,2,0) | + 0.487 | − 0.638 | + 0.751 | + 0.921 | − 1.027 | + 1.028 |
| (4,2,0) | + 0.495 | − 0.655 | + 0.718 | + 0.911 | − 1.115 | + 1.144 |
| (5,2,0) | + 0.498 | + 0.651 | − 0.707 | + 0.867 | − 1.181 | + 1.304 |
| $G(6,2,0)$ | 1 0.487 | 4 0.568 | 3 0.790 | 1 0.877 | 2 1.202 | 4 1.45 |
| $\Sigma(3,3,0)$ | 1 0.458 | 2 0.602 | 1 0.856 | 1 0.975 | 4 1.006 | 3 1.128 |
| (4,3,0) | + 0.455 | − 0.601 | + 0.854 | + 0.969 | + 1.104 | − 1.203 |
| $G(5,3,0)$ | 1 0.467 | 3 0.637 | 4 0.761 | 1 0.901 | 2 1.226 | 4 1.249 |
| $N(4,4,0)$ | 1 0.435 | 2 0.582 | 1′ 0.976 | 1 0.978 | 4 1.023 | 3 1.235 |
| $\Lambda(1,1,1)$ | 1 0.411 | 3 0.709 | 3 0.709 | 1 0.840 | 3 0.942 | 3 0.942 |
| (2,1,1) | + 0.466 | + 0.688 | − 0.688 | − 0.894 | + 0.910 | + 0.988 |
| (3,1,1) | + 0.522 | − 0.657 | + 0.705 | − 0.851 | + 0.985 | + 1.053 |
| (4,1,1) | + 0.561 | − 0.603 | + 0.734 | − 0.851 | + 1.032 | + 1.164 |
| (5,1,1) | − 0.541 | + 0.569 | + 0.746 | − 0.904 | + 1.078 | + 1.317 |
| (6,1,1) | − 0.488 | + 0.516 | + 0.809 | − 0.997 | + 1.123 | + 1.49 |
| $F(7,1,1)$ | 3 0.453 | 3 0.453 | 1 0.908 | 3 1.110 | 3 1.110 | 3 1.635 |
| (2,2,1) | + 0.499 | − 0.647 | + 0.686 | + 0.935 | − 0.976 | + 1.004 |
| (3,2,1) | 0.508 | 0.628 | 0.718 | 0.921 | 1.019 | 1.104 |
| (4,2,1) | 0.514 | 0.623 | 0.727 | 0.910 | 1.064 | 1.232 |
| (5,2,1) | 0.522 | 0.626 | 0.688 | 0.911 | 1.113 | 1.40 |
| (6,2,1) | + 0.514 | − 0.573 | + 0.714 | + 0.955 | − 1.132 | − 1.539 |
| (3,3,1) | + 0.484 | − 0.599 | + 0.808 | + 0.971 | − 1.009 | + 1.203 |
| (4,3,1) | 0.473 | 0.596 | 0.827 | 0.964 | 1.060 | 1.291 |
| (5,3,1) | + 0.491 | + 0.623 | − 0.752 | + 0.928 | − 1.122 | − 1.378 |
| $D(4,4,1)$ | 1 0.461 | 4 0.582 | 3 0.914 | 1 0.986 | 2 1.026 | 3 1.312 |
| $\Lambda(2,2,2)$ | 1 0.559 | 3 0.629 | 3 0.629 | 3 0.970 | 3 0.970 | 1 1.113 |
| (3,2,2) | + 0.556 | − 0.616 | + 0.674 | − 0.955 | + 1.015 | + 1.224 |
| (4,2,2) | + 0.544 | − 0.609 | + 0.720 | − 0.946 | + 1.044 | + 1.347 |
| (5,2,2) | + 0.567 | − 0.600 | + 0.680 | − 0.967 | + 1.056 | + 1.51 |
| $F(6,2,2)$ | 3 0.586 | 3 0.586 | 1 0.629 | 3 1.032 | 3 1.032 | 1 1.672 |
| (3,3,2) | + 0.553 | − 0.596 | + 0.722 | + 0.987 | − 1.014 | + 1.335 |
| (4,3,2) | 0.531 | 0.599 | 0.762 | 0.987 | 1.037 | 1.43 |
| (5,3,2) | + 0.539 | + 0.619 | − 0.722 | + 0.980 | − 1.049 | − 1.524 |
| $D(4,4,2)$ | 1 0.530 | 4 0.587 | 3 0.809 | 1 1.004 | 2 1.030 | 3 1.45 |
| $\Lambda(3,3,3)$ | 3 0.605 | 3 0.605 | 1 0.681 | 3 1.016 | 3 1.016 | 1 1.45 |
| (4,3,3) | + 0.575 | − 0.633 | + 0.710 | − 1.015 | + 1.031 | + 1.549 |
| $F(5,3,3)$ | 1 0.554 | 3 0.676 | 3 0.676 | 3 1.020 | 3 1.020 | 1 1.652 |
| $D(4,4,3)$ | 4 0.606 | 1 0.610 | 3 0.717 | 1 1.025 | 2 1.033 | 3 1.596 |
| $P(4,4,4)$ | 4 0.647 | 4 0.647 | 4 0.647 | 3 1.033 | 3 1.033 | 4 1.725 |

limited number of points in the Brillouin zone at which calculations have been carried out, this density-of-states would be necessarily crude. In order to obtain a more meaningful density of states, a simple interpolation scheme has been devised. This scheme approximates the $n$th-band eigenvalue for an energy-band state whose wave vector lies within a given cubic subzone by a weighted average of the $n$th-band APW eigenvalues at the cube corners. This method is such that along a cube edge, the interpolation is linear, on a cube face, it is planar, and at the cube center, the weighting factors are equal.

This interpolation scheme is admittedly poor along symmetry directions and in symmetry planes because it does not allow states with different symmetry to cross. However, as the mesh is reduced, a large proportion of wave vectors fall at general points in the Brillouin zone where such crossings are forbidden. Therefore, the results of such an interpolation scheme are expected to reproduce the gross features of the actual density of

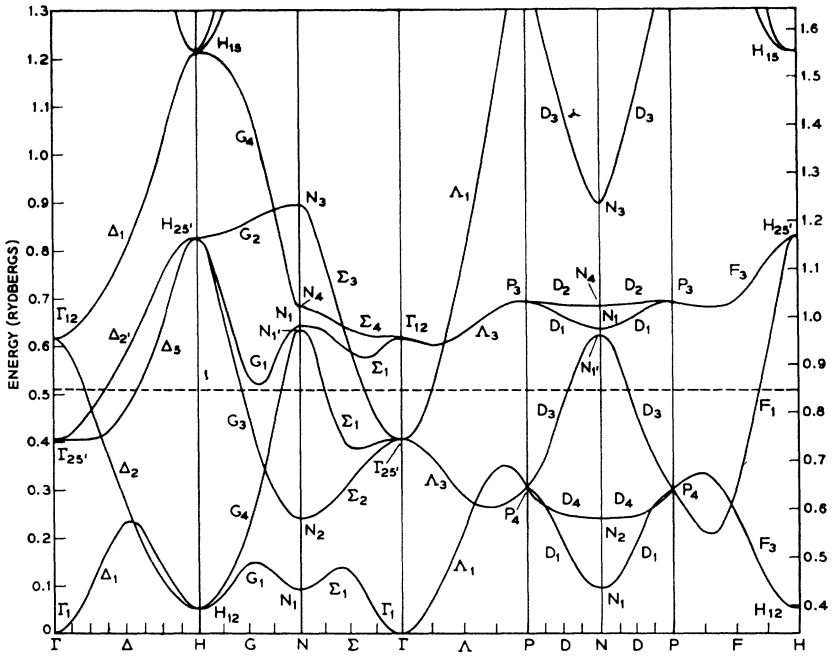


FIG. 3. Energy bands $E_1(\mathbf{k})$ along symmetry directions in the Brillouin zone for tungsten. The energy scale to the right corresponds to that of Table II. To the left, the zero of energy coincides with $E(\Gamma_1)$.

states. However, some of the peaks and singularities in the actual density of states may be broadened or washed out completely in the interpolation procedure.

The results of the density-of-states calculations for $W_1$ and $W_2$ are shown in Figs. 5 and 6, respectively. These figures result from calculations involving 221, 184 points in the Brillouin zone. Decreasing the total number of points to 65, 536 causes little change in the results. From Figs. 5 and 6, the Fermi energies for $W_1$ and $W_2$ are 0.850 and 1.155 Ry, respectively, as indicated by the dashed horizontal lines of Figs. 3 and 4, respectively.

Using the energy-band results tabulated in Table II, the nonrelativistic Fermi surfaces for $W_1$ and $W_2$ have been calculated in the (100) and (110) planes, and these are shown in Figs. 7(b) and 7(c), respectively. For comparison, the corresponding Fermi surface which results from Wood's iron calculations is drawn [7(a)], assuming

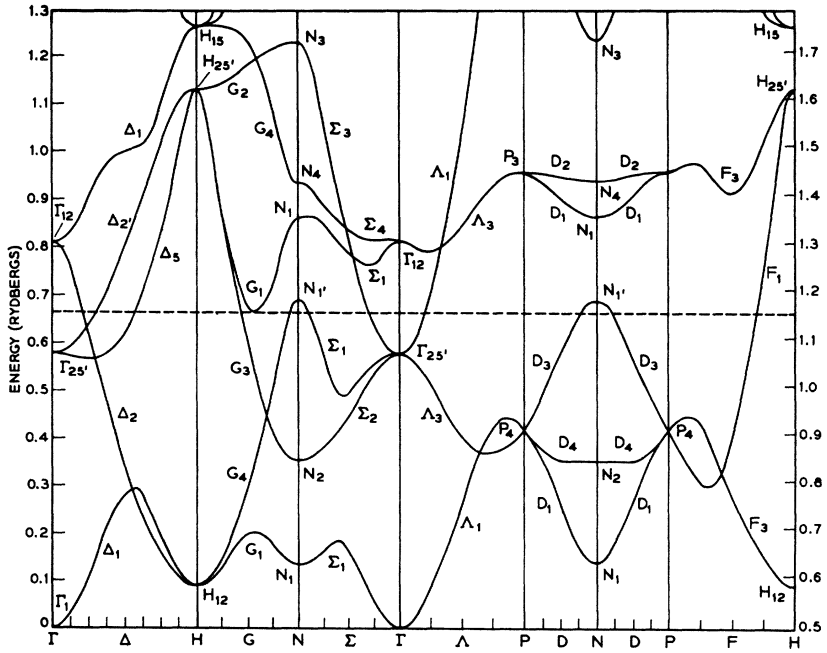


FIG. 4. Energy bands $E_2(\mathbf{k})$ along symmetry directions in the Brillouin zone for tungsten.

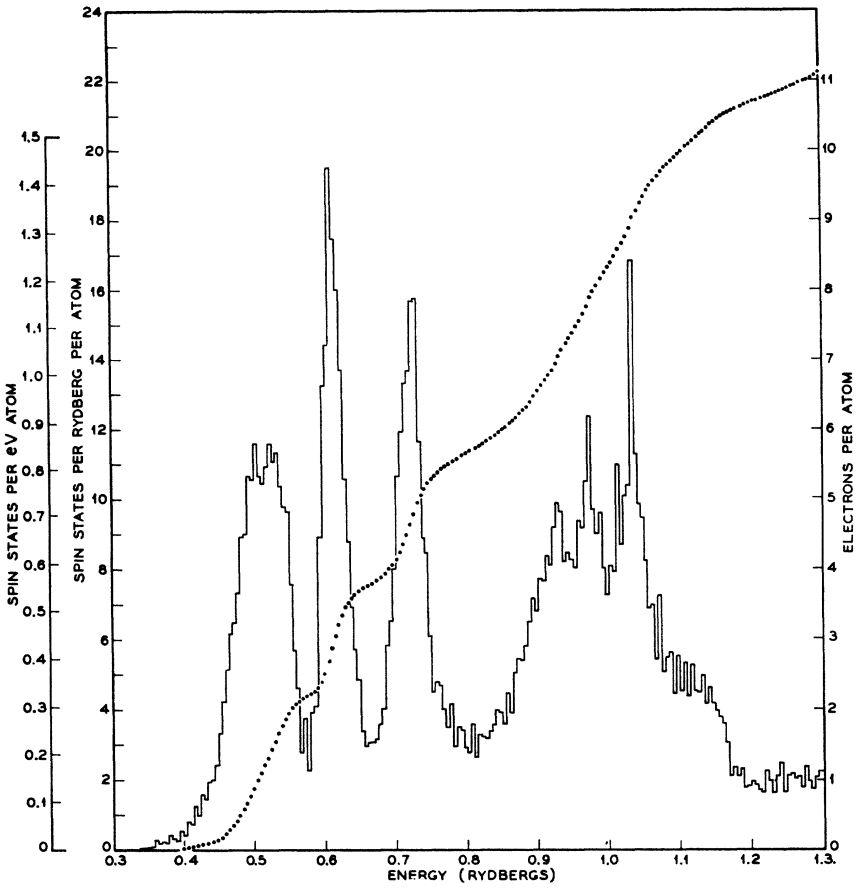


FIG. 5. Density-of-states curve for tungsten based on the $W_1$ results. The units to the left are states of one spin per eV atom and states of one spin/Ry atom. The dotted line is the integrated density of states; the corresponding units to the right are electrons per atom.

six occupied electronic states per atom. In computing the Fermi surfaces in Figs. 7(a), 7(b), and 7(c), graphical interpolation has been used along symmetry and nonsymmetry lines in the (100) and (110) planes to map out the Fermi surfaces as precisely as possible.

Convergence studies indicate that the APW eigenvalues for tungsten converge at approximately the same rate that Wood found in iron.[15] Sufficient APW basis functions have been included in the present calculations for tungsten to ensure convergence to 0.001 or 0.002 Ry at symmetry points, along symmetry lines, and in symmetry planes in the Brillouin zone. For convenience, the number of basis functions has been restricted for calculations at general points in the Brillouin zone such that these eigenvalues converge to approximately 0.004 Ry.

## IV. SPIN-ORBIT COUPLING

The size-effect results of Walsh and Grimes indicate that the electron "jack" and hole "octahedron" are separated by a gap along ⟨100⟩ which is equal to approximately 5% the $\Gamma\bar{H}$ distance. This gap has been attributed to spin-orbit splitting of the $\Delta_5$ state at the Fermi energy in tungsten.[18] By means of a simplified tight-binding calculation involving the present $W_1$ energy bands, it has been possible to estimate the $5d$ spin-orbit coupling parameter in metallic tungsten to be approximately 0.03 Ry (0.4 eV). A similar approach has been used by Friedel *et al.* to study spin-orbit effects in the face-centered cubic transition metals.[26]

The effects of spin-orbit coupling on the $W_1$ energy bands along $\Delta$ are shown in Fig. 8. In Fig. 8(a), the nonrelativistic results of Fig. 3 are replotted, using the double-group notation to label the various states.[27] From Fig. 8(a), it is clear that four energy bands cross the Fermi energy, three with $\Delta_7$ and one with $\Delta_6$ symmetry. The upper and lower $\Delta_6$ states would also cross the Fermi energy if they were not repelled by $s$-$d$ mixing.

It is possible to obtain a semiquantitative estimate of these spin-orbit effects by assuming tight-binding $5d$ wave functions for the $\Delta_{2'}$, $\Delta_5$, and $\Delta_2$ states. If it is further assumed that these $5d$ wave functions have the same radial function $P_{5d}(r)$, then the spin-orbit effects can be described in terms of a single spin-orbit parameter $\xi_{5d}$. Along ⟨001⟩, the $\Delta_{2'}$, $\Delta_5$, and $\Delta_2$ tight-binding wave functions can be characterized by the polynomials $xy(\Delta_{2'})$, $xz$, $yz(\Delta_5)$, and $(x^2-y^2)(\Delta_2)$, respec-

[26] J. Friedel, P. Lenglart, and G. Leman, J. Phys. Chem. Solids **25**, 781 (1964).
[27] R. J. Elliott, Phys. Rev. **96**, 280 (1954).

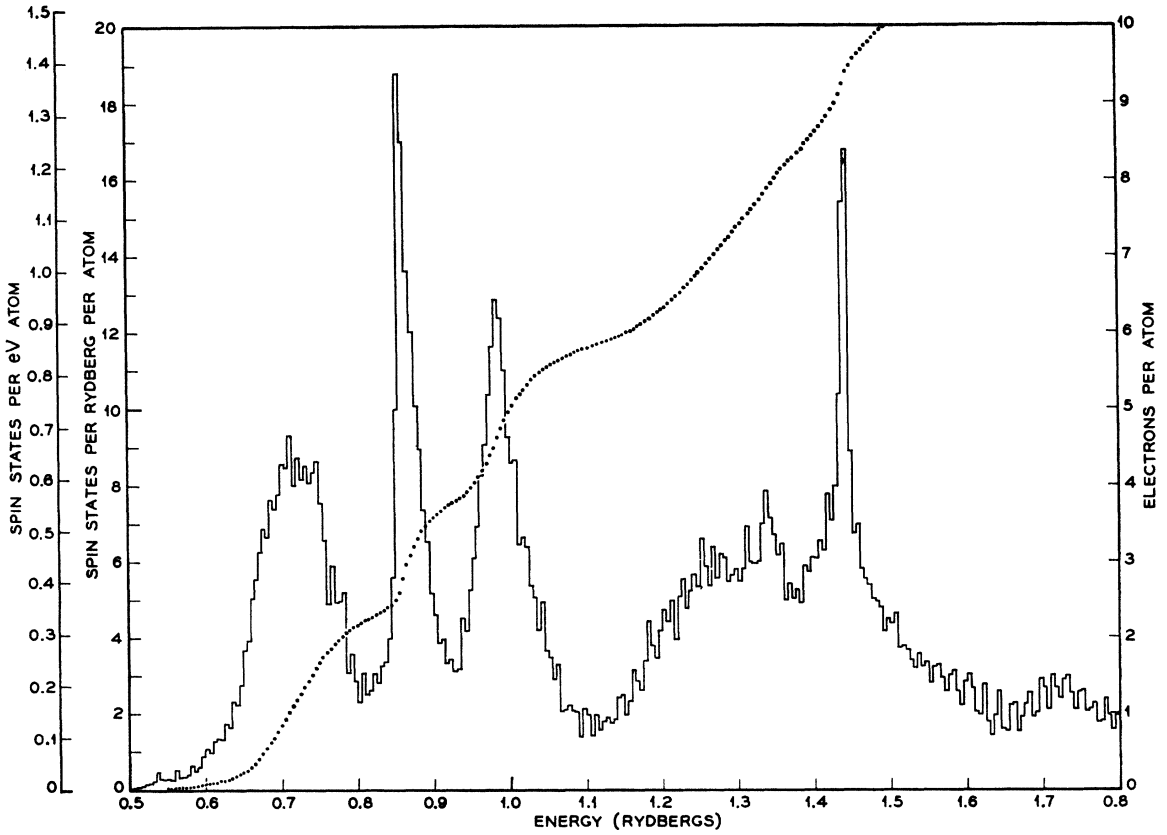


FIG. 6. Density of states for tungsten based on the $W_2$ results.

tively. Using the coupling coefficients tabulated by Koster *et al.*[28] to form functions which transform irreducibly under the double-group, it is straightforward to calculate diagonal and off-diagonal matrix elements of the spin-orbit operator $H_{so}=\xi(r)\mathbf{l}\cdot\mathbf{s}$ among these functions. Neglecting off-diagonal matrix elements, it is found that

$$\begin{aligned} E(\Delta_7)&=E(\Delta_5)+\tfrac{1}{2}\xi_{5d}, \\ E(\Delta_6)&=E(\Delta_5)-\tfrac{1}{2}\xi_{5d}. \end{aligned} \tag{1}$$

The corresponding calculation at $\Gamma$ (or $H$) yields the result

$$\begin{aligned} E(\Gamma_{7^+})&=E(\Gamma_{25'})+\xi_{5d}, \\ E(\Gamma_{8^+})&=E(\Gamma_{25'})-\tfrac{1}{2}\xi_{5d}. \end{aligned} \tag{2}$$

The Hamiltonian matrix for the $\Delta_7$ states has the following form when $\xi_{5d}\neq 0$:

$$\begin{vmatrix} E(\Delta_{2'}) & (\sqrt{2}/2)\xi_{5d} & -\xi_{5d} \\ (\sqrt{2}/2)\xi_{5d} & E(\Delta_5)+\tfrac{1}{2}\xi_{5d} & (\sqrt{2}/2)\xi_{5d} \\ -\xi_{5d} & (\sqrt{2}/2)\xi_{5d} & E(\Delta_2) \end{vmatrix}. \tag{3}$$

By means of a unitary transformation, this matrix can be reduced to its proper form at $\Gamma$ (or $H$):

$$\begin{vmatrix} E(\Gamma_{25'})+\xi_{5d} & 0 & 0 \\ 0 & E(\Gamma_{25'})-\tfrac{1}{2}\xi_{5d} & (\sqrt{6}/2)\xi_{5d} \\ 0 & (\sqrt{6}/2)\xi_{5d} & E(\Gamma_{12}) \end{vmatrix}. \tag{4}$$

The first row and column represent the $\Gamma_{7^+}$ state, while the remaining two rows and columns correspond to $\Gamma_{8^+}$ states. The corresponding matrix for the $\Delta_6$ states is complicated by *s-d* mixing. Since the $\Delta_6$ states do not cross, it is reasonable to assume that the effects due to off-diagonal spin-orbit matrix elements connecting the central $\Delta_6$ state with the upper and lower ones cancel approximately and can be neglected.

The three-by-three secular determinant for the $\Delta_7$ states has been solved as a function of $\xi_{5d}$. It has been found that the gap $\Delta k$ between the central $\Delta_6$ and $\Delta_7$ states at the Fermi energy is 5% the $\bar{\Gamma}\bar{H}$ distance when $\xi_{5d}$ is approximately 0.03 Ry. The results are shown in Fig. 8(b).

The upper $\Delta_7$ state barely crosses the Fermi energy when $\xi_{5d}\simeq 0.03$ Ry. This state produces the "lenses" within the "necks" of the electron "jack." Spin-orbit coupling reduces the size of these "lenses," separates these "lenses" from the "necks" in the (100) and (110) planes, and could cause the "lenses" to disappear

[28] G. F. Koster, J. O. Dimmick, R. G. Wheeler, and H. Statz, *Properties of the Thirty-Two Point Groups* (MIT Press, Cambridge, Massachusetts, 1963).

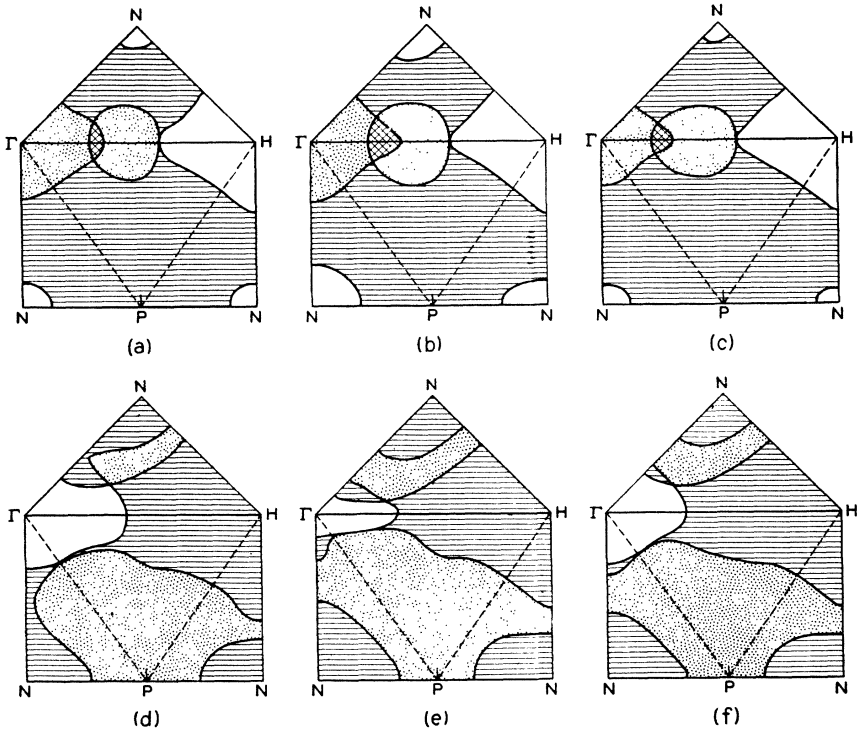


FIG. 7. Central (100) and (110) cross sections of the chromium- (a, b, c)- and vanadium-(d, e, f)-group Fermi surfaces, calculated using energy bands for iron (a, d), $W_1$(b, e), and $W_2$(c, f), respectively.

entirely in tungsten. However, spin-orbit coupling is not expected to have any other important consequences in tungsten as far as the topology of the Fermi surface is concerned.

## V. FERMI SURFACE IN VANADIUM-GROUP METALS

The fact that the three model Fermi surfaces in Figs. 7(a), 7(b), and 7(c) are qualitatively similar confirms Lomer's suggestion that the basic Fermi-surface topology for the chromium or group-VI transition metals is relatively insensitive to small changes in the band structure.[14] In the case of the group-V transition metals, the situation is somewhat more delicate since the Fermi energy is expected to fall near the energy-band state with $\Gamma_{25'}$ symmetry, $E(\Gamma_{25'})$. Small changes in the band structure could lead to vastly different Fermi surfaces. Experimental data for the group-V transition metals is limited, due to the lack of pure single crystals.

Nevertheless, it seems worthwhile to discuss the Fermi surface for group-V transition metals which results from the present nonrelativistic energy-band calculations for tungsten, especially since it is remarkably similar to the corresponding Fermi surface which is obtained from Wood's iron calculations.[15] Assuming a rigid-band model, the Fermi energies for the vanadium-group metals (as predicted from the present tungsten and previous iron calculations) lie slightly below $E(\Gamma_{25'})$. The corresponding Fermi surfaces are shown in Figs. 7(d), 7(e), and 7(f). These represent central sections of the (100) and (110) planes in the body-centered cubic Brillouin zone.

The topology of this Fermi surface is evident from the three-dimensional drawing in Fig. 9. The inner and

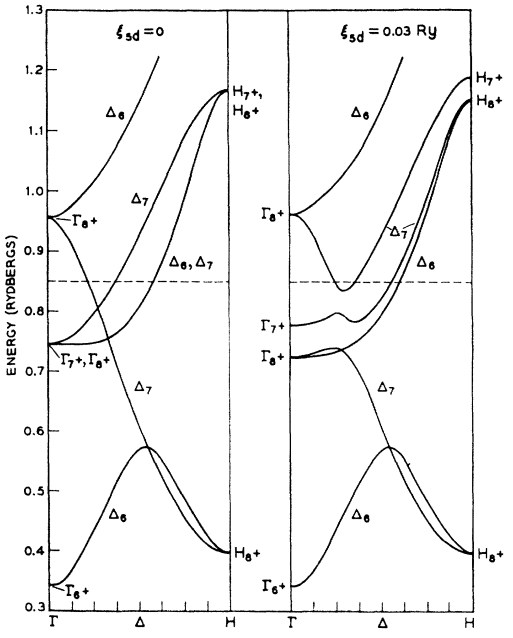


FIG. 8. Results of a simplified spin-orbit calculation along Δ for tungsten with $\xi_{5d}=0$ and 0.03 Ry.

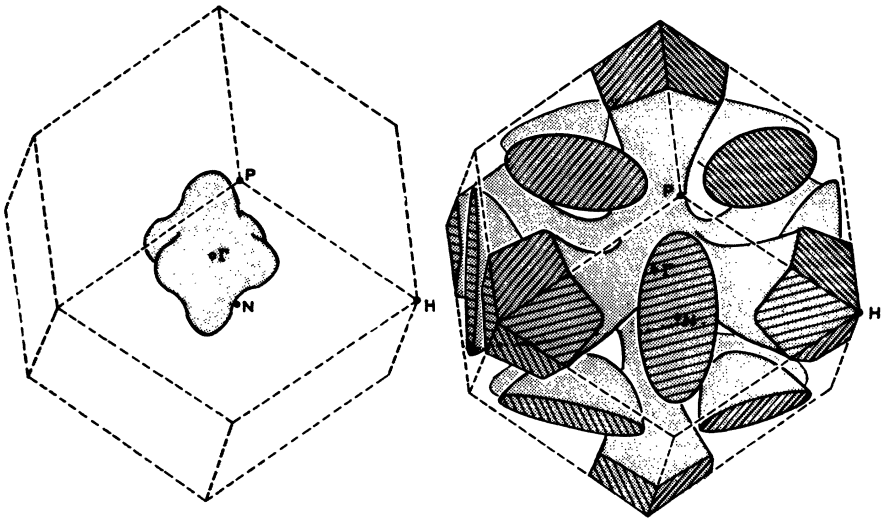


(a) (b)

FIG. 9. Proposed Fermi surface for the vanadium-group transition metals.

outer hole sheets are indicated in Figs. 9(a) and 9(b), respectively. The outer sheet consists of hole tubes along the ⟨100⟩ axes plus large ellipsoids at $N$. The iron results predict that these ellipsoids at $N$ are joined by necks along $\bar{\Gamma}\bar{N}$ to the outer hole surface. Otherwise, the three calculations predict qualitatively similar results.

From Figs. 7(d), 7(e), and 7(f) there are points of accidental degeneracy in the (100) and (110) planes where the inner closed hole sheet at Γ contacts the outer, multiply connected hole surface. These degeneracies will be removed by spin-orbit coupling. However, they could lead to magnetic breakdown in vanadium or niobium, where the spin-orbit coupling parameter is smaller.

In the previous section, it was shown that spin-orbit coupling reduces the sixfold $\Gamma_{25'}$ degeneracy, and splits this state into a doubly ($\Gamma_{7^+}$) and a fourfold ($\Gamma_{8^+}$) degenerate state. From Eq. (2), the energy of the $\Gamma_{8^+}$ state $E(\Gamma_{8^+})=E(\Gamma_{25'})-\frac{1}{2}\xi_{5d}$ if the off-diagonal matrix element connecting the two $\Gamma_{8^+}$ states is neglected. Therefore, spin-orbit splitting of the $\Gamma_{25'}$ state, which is presumably of the order of 0.03 Ry for the 5$d$ transition metals, could push $\Gamma_{8^+}$ below the Fermi energy in tantalum. In terms of Figs. 7(d), 7(e), and 7(f), this would extend the dotted region into Γ, producing a Fermi surface which consists of closed hole surfaces about $N$ and $H$ in the Brillouin zone.

Preliminary magnetoresistance measurements on tantalum by Fawcett and Reed indicate the likelihood of open orbits along the ⟨100⟩ directions, though this conclusion is only tentative at the present time.[29] In terms of the present model Fermi surface for the group-V transition metals, these results imply that $\Gamma_{8^+}$ remains above the Fermi energy in tantalum, and the Fermi-surface topology is qualitatively similar to that shown in Figs. 7(d), 7(e), 7(f), 9(a), and 9(b) with the accidental degeneracies removed by spin-orbit coupling. In addition, recent high-field Hall-effect measurements in normal niobium by Reed, Fawcett, and Kim[30] show that the density of carriers equals one hole per atom, a result which is also consistent with this model.

## VI. DISCUSSION OF THE RESULTS

The nonrelativistic energy bands for tungsten are very similar to those found previously using the APW method for the body-centered cubic 3$d$ transition metals,[15,20] aside from a substantial increase in the $d$ bandwidth. This increased bandwidth can be attributed to increased overlap of the 5$d$ functions. Comparing the Hartree-Fock-Slater atomic 3$d$ and 5$d$ wave functions for chromium and tungsten, respectively,[22] we find that the 5$d$ radial functions are more extended than the relatively compact 3$d$ functions. In order to determine the relative bandwidths for the 3$d$, 4$d$, and 5$d$ group-VI transition metals, limited APW calculations have been performed for (nonmagnetic) chromium and molybdenum, assuming $(d)^5(s)^1$ atomic configurations and using the methods described in Sec. II to calculate the corresponding potentials. Taking the energy difference $\Delta_d \equiv E(H_{25'})-E(H_{12})$ as a measure of the $d$ bandwidth, $\Delta_d$ values of 0.51, 0.68, 0.77, and 1.04 Ry are obtained for Cr(3$d$), Mo(4$d$), $W_1$(5$d$), and $W_2$(5$d$), respectively. The large difference between the $W_1$ and $W_2$ 5$d$ bandwidths indicates the extent to which this parameter depends on the potential.

The neglect of relativistic effects in the present energy-

[29] E. Fawcett and W. A. Reed (private communication).

[30] W. A. Reed, E. Fawcett, and Y. B. Kim (to be published).

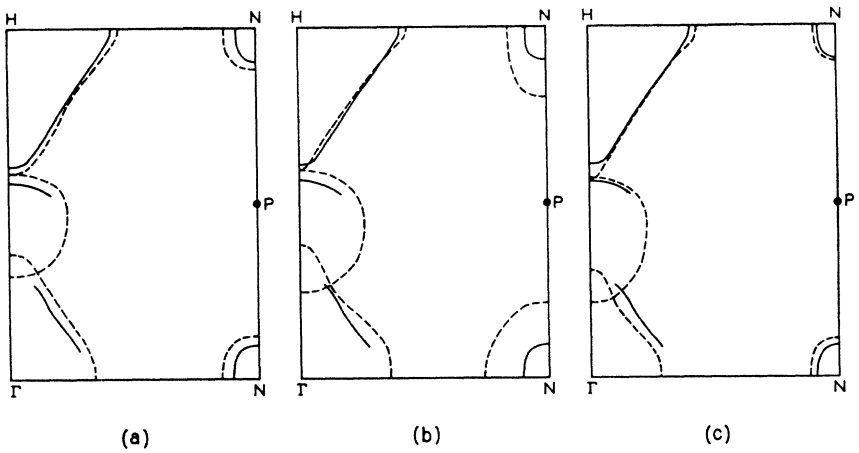


FIG. 10. Central (110) section of the tungsten Fermi surface, comparing the experimental dimensions (solid lines) with those calculated from the iron (a), $W_1$ (b), and $W_2$ (c) energy bands (dashed lines).

band calculations for tungsten represents a serious deficiency. Herman and Skillman have indicated the importance of mass-velocity and Darwin corrections in the heavier atoms.[22] Herman *et al.* have shown that these corrections for the outermost $s$ and $p$ electrons can be very large in tetrahedrally bonded semiconductors.[31] Clearly, these same corrections represent an important factor in determining the correct $s$-$d$ energy separation in metallic tungsten as well. Owing to the *ad hoc* nature of the potentials which have been used in the present calculations for tungsten, the uncertainty in the nonrelativistic $s$-$d$ energy separation is comparable in magnitude with these relativistic corrections. In view of this situation, it is reasonable to neglect these relativistic corrections. However, it is necessary to keep in mind that any detailed agreement between theory and experiment could be fortuitous, owing to cancellation of errors.

It would be interesting to apply the Slater-Koster tight-binding interpolation scheme[32] to tungsten since the simplified treatment of spin-orbit coupling that is described in Sec. IV could then be applied at more general points in the Brillouin zone. Our attempts to apply this method to the tungsten energy bands indicate that a large number of parameters would be required in order to obtain an accurate fit. For example, if five tight-binding parameters are chosen to fit the state with $\Delta_5$ symmetry at $\Gamma$, $H$, and three evenly spaced points along $\Delta$ in the $W_1$ calculations, the tight-binding results at the remaining points along $\Delta$ differ from the APW results by as much as 0.01 Ry. This implies that either a large number of tight-binding parameters are required to fit the tungsten $5d$ bands or the shape of the $\Delta_5$ band is affected by $6p$-$5d$ interactions. The latter alternative would complicate the simplified treatment of spin-orbit coupling that is presented in Sec. IV and vitiate our estimate of the spin-orbit parameter $\xi_{5d}$.

[31] F. Herman, C. D. Kuglin, K. F. Cuff, and R. L. Kortum, Phys. Rev. Letters **11**, 541 (1963).
[32] J. C. Slater and G. F. Koster, Phys. Rev. **94**, 1498 (1954).

Comparisons between the theoretically and experimentally determined Fermi surfaces in tungsten do not test critically the accuracy of the present calculations. This is clear from Figs. 7(a), 7(b), and 7(c), where the nonrelativistic Fermi surface is found to be rather insensitive to the $d$ bandwidth. There are some features of the Fermi surface which provide indirect information about the $5d$ bandwidth and the $s$-$d$ energy separation in tungsten. However, accurate relativistic calculations, including spin-orbit coupling, would be required in order to extract this information reliably.

The most useful experimental information about the larger pieces of Fermi surface in tungsten have been obtained by Walsh and Grimes, using the size-effect technique.[12] Their results, which map out the linear dimensions of portions of the electron "jack" and the entire hole "octahedron" in a (110) plane in tungsten, are indicated by the solid lines in Fig. 10. These size-effect results are in excellent agreement with the recent magnetoacoustic data of Jones and Rayne.[6] The ellipsoids at $N$ are also drawn in with solid lines in Fig. 10, using the dimensions obtained by Sparlin from his de Haas–van Alphen results.[17] The dashed lines in Fig. 10(a) represent the Fermi surface for chromium-group metals that is obtained from Wood's iron calculations.[15] The corresponding dashed lines in Figs. 10(b) and 10(c) are the Fermi surfaces obtained from the present $W_1$ and $W_2$ calculations, respectively.

The agreement between the measured and calculated Fermi surface dimensions in the (110) plane is fairly good. As described in Sec. IV, the fact that the electron "jack" and hole "octahedra" fail to touch along $\Delta$ is readily explained in terms of spin-orbit coupling. Spin-orbit coupling also causes the "lenses" inside the "necks" of the electron "jack" (which are omitted from Fig. 10) to be reduced in size and perhaps removed entirely in tungsten.

The dimensions of the hole ellipsoids at $N$ are determined by the energy difference between $E(N_{1'})$ and the Fermi energy. Since $N_{1'}$ is primarily a $6p$ state, this energy difference depends on the energy separation

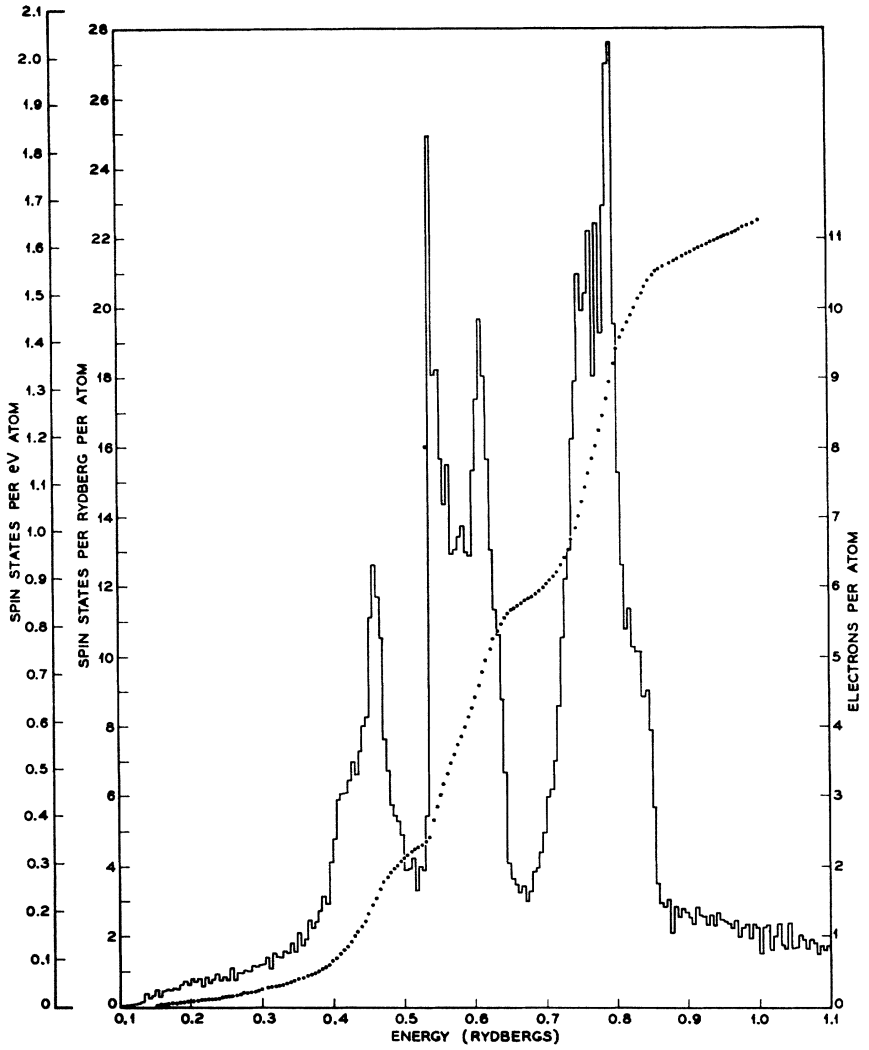


FIG. 11. Density of states for iron based on Wood's energy-band results.

between the $s$-$p$ and $d$ bands. In the $W_1$ calculation, $E(N_{1'})$ is approximately 0.13 Ry above the Fermi energy and the dimensions of these ellipsoids are large. In the $W_2$ calculation, this energy difference has been reduced to 0.025 Ry with a corresponding reduction in the ellipsoid dimensions. Sparlin has deduced that the major axis of these ellipsoids is along $\langle 100 \rangle$, with the minor axes along $\langle 110 \rangle$.[17] This result is consistent with the present calculations, which also predict that the larger and smaller of the minor axes are in the $\bar{\Gamma}\bar{N}$ and $\bar{H}\bar{N}$ directions, respectively.

Assuming parabolic bands and using experimentally determined cyclotron masses, Sparlin has estimated that $E(N_{1'})$ is approximately 0.28 eV (0.02 Ry) above the Fermi energy in tungsten. Using either the $W_1$ or $W_2$ energy-band results, a surface of constant energy which is 0.02 Ry below $E(N_{1'})$ predicts axes for the general ellipsoids which are within a few percent of the values obtained by Sparlin.

According to Fig. 7, the dimensions and shape of the hole "octahedron" at $H$ are relatively insensitive to the details of the band structure. This is not true for the electron "jack" at $\Gamma$. Changes in the $s$-$d$ energy separation and the $d$ bandwidth affect the relative sizes of the octahedral body and the balls which make up this "jack." It is found that the position of the "neck" along $\Delta$ is approximately proportional to the $d$ bandwidth. The size-effect results suggest that a plane through a "neck" intersects the $\Delta$ axis at a distance from $\Gamma$ which is 27% of the $\bar{\Gamma}\bar{H}$ distance. In terms of the present nonrelativistic results, this implies that the actual $5d$ bandwidth in tungsten is closer to that predicted by the $W_1$ rather than the $W_2$ calculations.

An accurate calculation of the cyclotron masses for orbits on the larger pieces of Fermi surface in tungsten is difficult due to the small number of points in the Brillouin zone at which energy-band results have been obtained. Although graphical interpolation is adequate

for estimating Fermi-surface dimensions and areas in a given plane, the rate of change of area is more difficult to estimate using these techniques.

An approximate calculation of the cyclotron mass has been made for the extremal orbit around the hole "octahedron" at $H$ with the magnetic field in a $\langle 100 \rangle$ direction. The calculated values for $m_c/m_0$ are found to be 0.93 and 0.82 for $W_1$ and $W_2$, respectively, with an estimated error of about 10%. These masses have been measured by Walsh[33] and Sparlin,[17] who find values of 1.02 and 1.06–1.11, respectively. By comparison, Wood's energy bands for iron predict $m_c/m_0 \simeq 1.63$. Whether the discrepancies between the calculated and experimental values for this cyclotron mass are due to the neglect of relativistic effects, overestimation of the $5d$ bandwidth, or electron-phonon effects is still uncertain.

The similarity between the density of states for $W_1$ (Fig. 5) and $W_2$ (Fig. 6) suggests that the gross features of the density-of-states curves for body-centered cubic transition metals are only slightly affected by appreciable changes in the $d$ bandwidth. This similarity is further reflected by the density-of-states curve for iron which is shown in Fig. 11. This density of states has been calculated using the interpolation procedure that is described in Sec. III and Wood's energy-band results. This density of states for iron is similar to one obtained by Wohlfarth and Cornwell,[34] which also was based on Wood's results. However, Wohlfarth and Cornwell fitted these results using the tight-binding interpolation scheme. Using thirty parameters to represent the $4s$, $4p$, and $3d$ bands, Wohlfarth and Cornwell have calculated a density of states which exhibits many sharp peaks. Most of this fine structure in the density of states has been presumably lost in the present calculation as a result of the relatively crude interpolation procedures that have been used.

Assuming a rigid-band density-of-states model for the body-centered cubic transition metals, the combined results of Figs. 5, 6, and 11 suggest that there are three peaks in the density of states below the Fermi energy for the group-VI transition metals. Above the Fermi energy, there is a relatively broad peak, with a fairly sharp spike near the top of the $d$ band. Measurements of the specific-heat coefficients $\gamma$ for the $3d$, $4d$, and $5d$ transition metals and alloys by Cheng *et al.*,[35] Morin and Maita,[36] and Bucher *et al.*,[37] respectively, indicate the presence of the first peak in the density of states below the group-VI Fermi energy. Outside this range, structure changes prevent any detailed comparisons with experiment.

In the case of tungsten, a recent measurement of $\gamma$ by Maita, using a sample with a resistivity ratio of 20 000, has been reported by Geballe.[38] Maita finds $\gamma = 2.0 \times 10^{-4}$ cal/mole$^{-1}$ deg$^{-2}$, which corresponds to a density of states at the Fermi energy $N(0) = 0.18$ states of one spin/eV atom. This result is in fair agreement with the values of approximately 0.28 and 0.16 states of one spin/eV atom that are obtained from the present $W_1$ and $W_2$ calculations, respectively.

In conclusion, the fact that these nonrelativistic energy-band results for tungsten are in good qualitative agreement with experiment leads to the hope that approximate energy bands and Fermi surfaces for other $5d$ transition metals can be calculated nonrelativistically. However, preliminary calculations for hexagonal rhenium indicate a rather complicated Fermi surface which could be severely modified by spin-orbit and other relativistic corrections.

*Note added in proof.* The results of relativistic energy-band calculations for tungsten, [T. L. Loucks, Phys. Rev. Letters **14**, 693 (1965)], are in good qualitative agreement with the present results.

## ACKNOWLEDGMENTS

The author is grateful to W. M. Walsh, Jr. and J. H. Condon for helpful discussions regarding the experimental results and their interpretation. He is indebted to J. H. Wood for providing the APW programs that have been used in this investigation.

[33] W. M. Walsh, Jr. (private communication).
[34] E. P. Wohlfarth and J. F. Cornwell, Phys. Rev. Letters **7**, 342 (1961).
[35] C. H. Cheng, C. T. Wei, and P. A. Beck, Phys. Rev. **120**, 426 (1960).
[36] F. J. Morin and J. P. Maita, Phys. Rev. **129**, 1115 (1963).
[37] E. Bucher, F. Heiniger, and J. Muller, Proceedings of the Ninth International Conference on Low Temperature Physics, Columbus, 1964 (to be published).
[38] T. H. Geballe, Rev. Mod. Phys. **36**, 134 (1964).

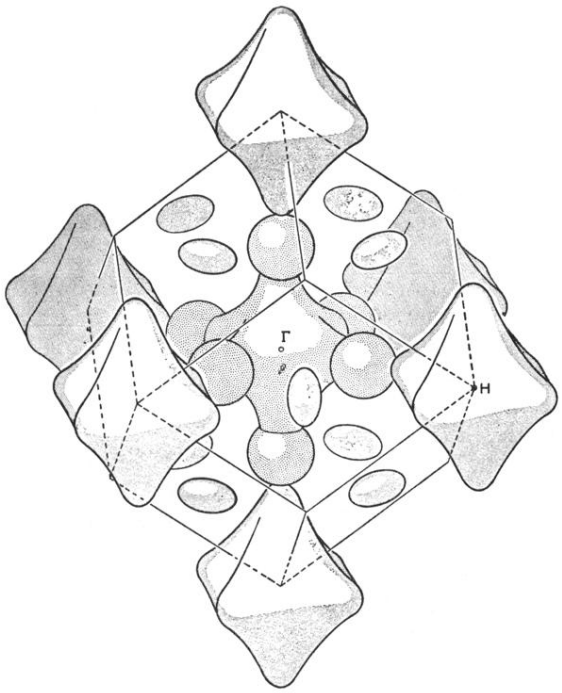


FIG. 1. A three-dimensional stretch of Lomer's revised Fermi surface for chromium-group metals.

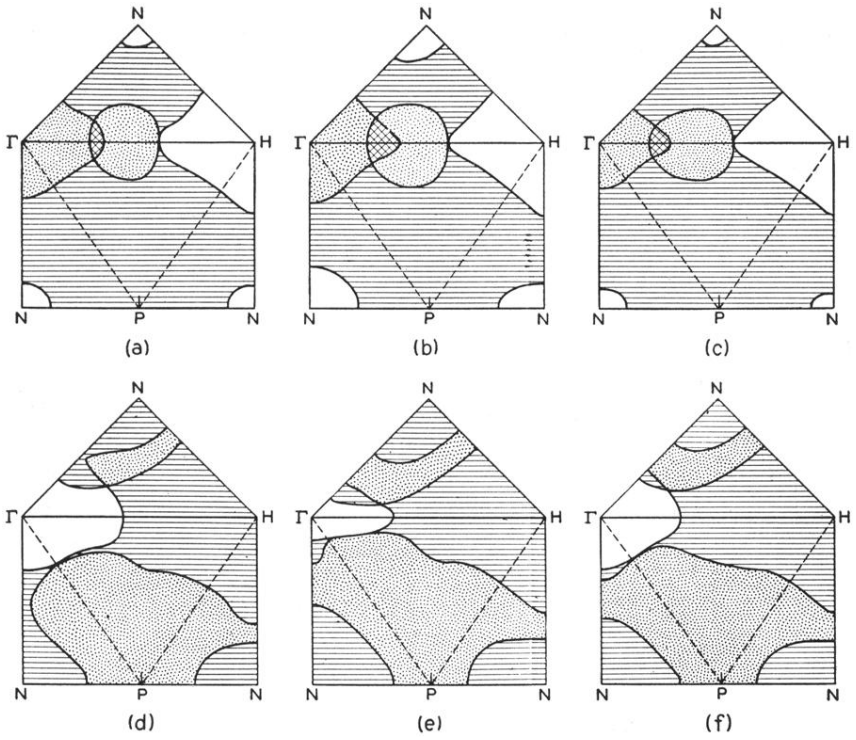


FIG. 7. Central (100) and (110) cross sections of the chromium- (a, b, c)- and vanadium-(d, e, f)-group Fermi surfaces, calculated using energy bands for iron (a, d), $W_1$(b, e), and $W_2$(c, f), respectively.

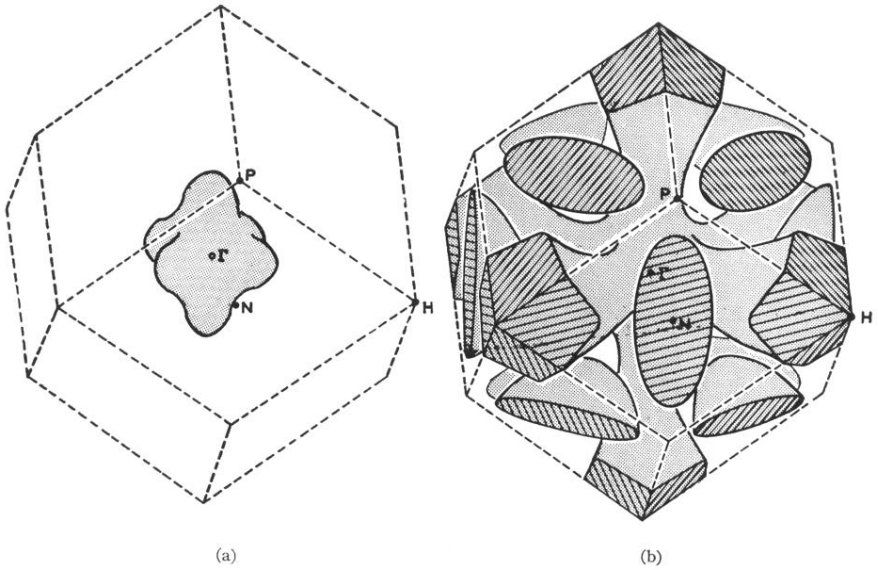


(a) (b)

FIG. 9. Proposed Fermi surface for the vanadium-group transition metals.